

# Gamma-rays flashes from dark photons in neutron star mergers

Melissa Diamond<sup>1,\*</sup> and Gustavo Marques-Tavares<sup>2,†</sup>

<sup>1</sup>*Department of Physics and Astronomy, Johns Hopkins University, Baltimore, MD 21218, U.S.A.*

<sup>2</sup>*Maryland Center for Fundamental Physics, Department of Physics, University of Maryland, College Park, MD 20742, U.S.A.*

In this letter we begin the study of visible dark sector signals coming from binary neutron star mergers. We focus on dark photons emitted in the 10 ms - 1 s after the merger, and show how they can lead to bright transient gamma-ray signals. The signal will be approximately isotropic, and for much of the interesting parameter space will be close to thermal, with an apparent temperature of about 100 keV. These features can be used to distinguish the dark photon signal from the expected short gamma-ray bursts produced in neutron star mergers, which are beamed in a small angle and non-thermal. We calculate the expected signal strength and show that for dark photon masses in the 1 – 100 MeV range it can easily lead to total luminosities larger than  $10^{46}$  ergs for much of the unconstrained parameter space. This signal can be used to probe a large fraction of the unconstrained parameter space motivated by freeze-in dark matter scenarios with interactions mediated by a dark photon in that mass range. We also comment on future improvements when proposed telescopes and mid-band gravitational detectors become operational.

## I. INTRODUCTION

The detection of gravitational waves (GW) from binary neutron star (BNS) mergers, and the observation of their electromagnetic counterparts has inaugurated a new era in multi-messenger astronomy [1–3]. With upcoming observations we will learn more about the physics of neutron stars, the origin of heavy elements and models of stellar evolution [4–7]. This new window into the universe offers great potential as a probe of physics beyond the standard model (BSM), in particular of scenarios involving very weakly interacting new states.

In the merger of two neutron stars, a meta-stable remnant is formed with nuclear densities and temperatures in the 10s of MeV, similar to the proto-neutron stars formed in core-collapse supernovae [8–11]. For a brief period of time, these remnants are one of the densest and hottest regions in the universe, and hence a promising source of new weakly coupled particles. In fact, it has been shown that such events can produce a large flux of neutrinos [12]. Nonetheless, the low rate of mergers implies that if we are interested in seeing at least  $\mathcal{O}(1)$  event/year, their typical distance will be  $\sim 100$  Mpc, making direct observation of the new particles challenging due to their small flux at large distances and small couplings. If, on the other hand, the new particles are unstable and can decay to visible particles, such as leptons or photons, they can produce very bright signals and make BNS mergers a powerful probe of new physics scenarios.

There have been a number of proposals to search for

new physics affecting the gravitational wave signal from binary black-holes and neutron stars [13–20], in addition to potential cooling constraints due to emission of weakly coupled BSM particles from the remnant [21, 22]. In this letter, we initiate the study of dark sector electromagnetic signals in BNS mergers.

For concreteness, we will focus exclusively on dark photons, even though this framework can be applied to many dark sector models with unstable particles. The dark photon is a new massive vector field that kinetically mixes with the photon, and through this mixing interacts with charged standard model matter [23, 24]. It corresponds to one of the three renormalizable portals between the Standard Model (SM) and dark sectors, which are sectors not charged under the standard model gauge group [25, 26]. Dark matter might be part of such a dark sector, and its interactions with the standard model mediated by the dark photon can account for the observed dark matter density. The relic abundance can be obtained either through standard freeze-out, corresponding to scenarios in which dark matter reaches full thermal equilibrium with the visible sector and requires larger couplings, or through freeze-in in which the interactions are so weak that dark matter never gets to thermal equilibrium with the SM [27, 28].

The sizeable cross-sections suggested by the freeze-out scenario motivated a large experimental program aiming to cover the parameter space corresponding to the observed relic density. The freeze-in scenario, on the other hand, points to a tiny coupling, with the kinetic mixing parameter as small as  $10^{-11}$ , making it much more difficult to probe experimentally. There are a number of recent direct detection proposals that aim to reach the freeze-in parameters in the limit of very light dark photons, taking advantage of the cross-section enhancement

---

\*Electronic address: mdiamond8@jhu.edu

†Electronic address: gusmt@umd.edu

at low velocities characteristic of interactions mediated by light particles (e.g. [29–32]). The prospects for probing the freeze-in scenario for larger dark photon masses, when there is no significant enhancement of the cross-section, are much more challenging. Many of the constraints on this scenario come from searches that are sensitive to the dark photon directly, in most cases using cosmological or astrophysical signals [33–39]. We will show that dark photons in the mass range  $\sim 1 - 100$  MeV can be produced copiously in the remnant of a neutron star merger. Their decays lead to a transient bright gamma-ray signal that can be used to search for dark photons in much of the remaining viable parameter space for freeze-in with mediator mass in the MeV to GeV range.

## II. DARK PHOTON PRODUCTION AND DECAY

We will concentrate on dark photon production and assume that any other new particle charged under the dark photon is sufficiently heavy so that it will not play a role in neutron star mergers (which effectively requires charged states to be heavier than about 100 MeV). In this case the relevant terms in the lagrangian are

$$\mathcal{L} \supset \frac{1}{2} m' A'_\mu A'^\mu - \frac{1}{4} F'_{\mu\nu} F'^{\mu\nu} - \frac{\epsilon}{2} F'_{\mu\nu} F^{\mu\nu}, \quad (1)$$

where  $A'^\mu$  is the dark photon,  $m'$  its mass,  $F'^{\mu\nu}$  the photon field strength, and  $\epsilon$  the kinetic mixing.

The production of dark photons in the proto-neutron star is dominated by nucleon-nucleon bremsstrahlung, as in the supernova case. The flux of dark photons can be calculated following Ref. [37] and is given by

$$\frac{dN}{dV dt} = \int \frac{d\omega \omega^2 v}{2\pi^2} e^{-\omega/T} (\Gamma_{\text{abs},L} + 2\Gamma_{\text{abs},T}), \quad (2)$$

where  $\omega$  is the frequency of the dark photon,  $v$  its velocity,  $T$  the temperature of the region and  $\Gamma_{\text{abs},T/L}$  the absorption width for the transverse/longitudinal dark photon modes. This is multiplied by the volume of the emitting region and the emission time to get the total number of dark photons produced. The absorption width can be computed using the soft-radiation approximation, as discussed in Ref. [40]. Ignoring Pauli blocking for simplicity (which is at most an  $\mathcal{O}(1)$  effect), we find

$$\Gamma_{\text{abs}, X} = \frac{32\alpha n_n n_p \epsilon^2 m'^4}{3\pi\omega^3 ((m'^2 - \text{Re}\Pi_X)^2 + \text{Im}\Pi_X^2)} \left(\frac{\pi T}{m_N}\right)^{3/2} \times \langle \sigma_{\text{np}}^{(2)}(T) \rangle \times \begin{cases} 1, & X = T \\ (m'/\omega)^2, & X = L \end{cases}, \quad (3)$$

where  $X = T/L$  refers to the polarization of the dark photon,  $m_N$  is the nucleon mass,  $n_{n/p}$  is the neutron/proton density,  $\Pi_X$  is the in medium polarization tensor of the photon (see Supplementary Materials for

their explicit form) and  $\langle \sigma_{\text{np}}^{(2)} \rangle$  is the weighted proton neutron scattering cross-section taken from Ref. [40]. From Eq. 2 we can calculate the dark photon luminosity

$$\frac{dE}{dV dt} = \int \frac{d\omega \omega^3 v}{2\pi^2} e^{-\omega/T} (\Gamma_{\text{abs},L} + 2\Gamma_{\text{abs},T}). \quad (4)$$

Based on BNS merger simulations in Ref. [9–11, 41], we assume a simplified, spherically symmetric description of the merger remnant, with a constant temperature, density and electron fraction:  $T = 30$  MeV,  $\rho = 4 \times 10^{14}$  g cm $^{-3}$ ,  $Y_e = 0.1$  in the region 5 km-10 km from the center of the remnant. We consider only the dark photons produced in this hotter region and ignore contributions from other lower temperature regions.

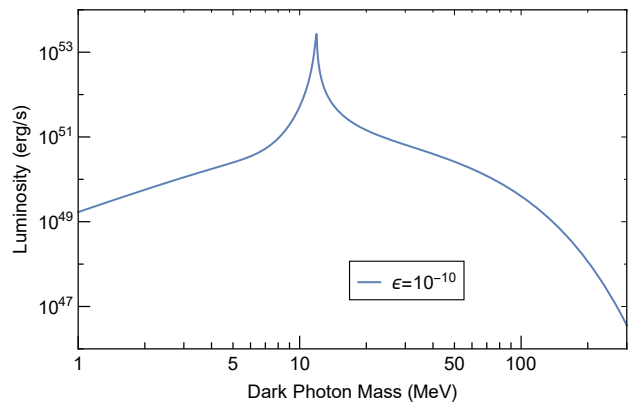


FIG. 1: Luminosity of dark photons with  $\epsilon = 10^{-10}$  produced in a BNS merger. The luminosity scales as  $\epsilon^2$  for all masses and the enhancement near 10 MeV is due to resonant mixing between the dark photon and the photon.

The time evolution of the remnant depends on the mass of the binary neutron stars and the equation of state of nuclear matter. Different initial conditions can produce a variety of different remnants that persist for between 1 – 1000 ms before collapsing to a black hole [8–11, 41]. Light remnants might even not collapse at all, giving rise to a heavier neutron star [42]. Nonetheless, due to cooling, their temperature will decrease from  $T \sim 30$  MeV in a few seconds timescale [21, 43]. In order to illustrate this range of possibilities, we will present results assuming two scenarios: dark photon emissions lasting 10 ms after the merger and emissions lasting 1 s after the merger. Note that most analysis of GW170817 conclude that the remnant must have lasted for at least 10 ms [44–47]. Finally, for simplicity we will ignore the impact of gravitational redshift, which depends strongly on the density distribution in the central region of the merger (we estimate the impact of this effect in the Supplementary Material III). In Fig. 1 we show the dark photon luminosity using the merger parameters described right after Eq. 4 for  $\epsilon = 10^{-10}$ .

After production, the dark photons decay to electron-positron pairs, leading to an expanding plasma shell. The

dark photon decay width at rest is

$$\Gamma = \frac{1}{3}\alpha\epsilon^2 m' \sqrt{1 - \frac{4m_e^2}{m'^2}} \left(1 + \frac{2m_e^2}{m'^2}\right), \quad (5)$$

where  $m_e$  is the electron mass. The initial Lorentz factor of the expanding shell is approximately the average Lorentz factor of the dark photon flux,

$$\gamma_0 = \frac{\langle\omega\rangle}{m'}, \quad (6)$$

where  $\langle\omega\rangle$  is the average dark photon energy. In the merger frame, the dark photon decay length is

$$d = \frac{\gamma_0 v}{\Gamma}, \quad (7)$$

where  $v$  is the dark photon velocity. The width of the plasma shell immediately after the decay is

$$\delta = \frac{1}{\gamma_0 \Gamma}, \quad \delta' = \frac{1}{\Gamma} \quad (8)$$

in the star frame and plasma frame respectively.

The photon signal we are interested in depends on the evolution of this plasma. Large baryon density and magnetic fields in the decay region would lead to many complications in modeling the plasma evolution. For this reason, we focus on parameters such that the dark photon decay distance is at least 1000 km from the center of the merger, at which point baryon density and magnetic fields can be safely neglected. When calculating the number of leptons that results from dark photon decays, we only include the fraction coming from decays 1000 km or more from the merger. Most of the parameter space that is not constrained by other bounds already leads to sufficiently long decay lengths, and so this requirement does not lead to a significant change in sensitivity.

### III. GAMMA-RAY SIGNAL

We are interested in photon signals arising from the electrons and positrons produced by the dark photon decay. With our simplified approximation for the proto-neutron star, the signal will be isotropic<sup>1</sup>, peaked between 100 keV and 10s of MeV and visible within about a second of the merger. The isotropic nature of the signal, its duration and the spectral information can be used to distinguish the signal from the short gamma-ray burst (GRB) expected to be produced from relativistic jets after the remnant collapses to a black hole [3, 48].

We will track the dynamics of the plasma starting out at a radius equal to the decay length of the dark photon

in the star frame, given by Eq. 7. In order to describe the properties of the plasma, we define quantities in the co-expanding frame, in which the lepton momenta distribution is isotropic and initially is related to the merger frame by a Lorentz factor given by Eq. 6. In this frame, the initial temperature is directly related to the dark photon mass,  $T \approx m'/6$ , since in that frame each electron and positron generated by the dark photon has approximately  $m'/2$  energy, with a small spread related to the dark photon boost distribution. The initial number density is given by

$$n_e \approx \frac{N_{\text{tot}}\gamma_0}{8\pi d^3}. \quad (9)$$

Similarly to the standard fireball model [48, 49], as long as the plasma energy is dominated by relativistic particles, the density evolves as  $\rho \propto r^{-4}$ , where  $r$  is the distance of the plasma shell from the remnant (in the remnant's rest frame), the Lorentz factor of the shell increases as  $\gamma \propto r$ , and the width in the merger frame which also determines the duration of the signal remains constant. If there are no processes that can change the total number density besides the expansion, the total number particle number is conserved and the total number density scales as  $n \propto r^{-3}$ , from which it follows that the temperature goes as  $T \propto r^{-1}$ .

The electron/positron densities in the plasma can be sufficiently large for pair annihilation,  $e^+e^- \rightarrow \gamma\gamma$ , to be very efficient. In this case, the pair creation and annihilation processes quickly leads the number densities of electrons and photons to be related by detailed balance,

$$\frac{n_e}{n_\gamma} = \frac{n_e^{\text{eq}}}{n_\gamma^{\text{eq}}}, \quad (10)$$

where the RHS of this equation refers to the equilibrium number densities for leptons and photons. In this regime, the photon mean free path will be short and the plasma is optically thick. An observable signal emerges once the lepton number density becomes sufficiently low for the plasma to become optically thin, allowing photons to escape. In addition to pair creation/annihilation, the other process that plays an important role in the dynamics of the plasma is photon bremsstrahlung from electron and positron scattering. While pair creation/annihilation preserves the total number of particles, since it is a 2 to 2 process, bremsstrahlung increases the total number of particles and consequently the total number density. Energy conservation implies that the temperature decreases as the number density goes up, and thus bremsstrahlung can lower the peak energy of the photon signal.

To determine if pair annihilation and bremsstrahlung are important effects, we compare their rates in the plasma frame to the number density dilution rate coming from the expansion,

$$\Gamma_{\text{exp}} = -3\gamma/r. \quad (11)$$

<sup>1</sup> In a realistic scenario the remnant is not spherically symmetric and there will be  $\mathcal{O}(1)$  variations in the luminosity depending on the inclination angle with respect to the plane of the merger.

The rate for pair annihilation is given by [50]

$$\Gamma_{\text{annih}} \approx \frac{\pi n_e \alpha^2}{m_e^2} \left( 1 + \frac{2(T/m_e)^2}{1 + \log\left(\frac{2T}{m_e e^{\gamma_E}} + 1.3\right)} \right)^{-1}, \quad (12)$$

where  $\gamma_E$  is the Euler-Mascheroni constant. The photon production rate from  $e^+e^-$  bremsstrahlung in a relativistic gas ( $T \gg m_e^2$ ) is [51]

$$\Gamma_{\text{brem}} \approx \frac{2n_e \alpha^3 \log(e^{\gamma_E} m_e^2/T^2)}{9m_e^2} [12 \log(e^{\gamma_E} m_e^2/T^2) - 84 + 48 \log(e^{\gamma_E} m_e/T)], \quad (13)$$

where we imposed an infrared cutoff on the photon energy  $\omega > m_e^2/T$ , corresponding to photons that can exchange  $\mathcal{O}(T)$  of energy in a single Compton scattering and thus quickly thermalize. For  $T \lesssim 1$  MeV, we switch to the non-relativistic rate [52]

$$\Gamma_{\text{brem}} \approx \frac{64}{3\sqrt{\pi}} \frac{n_e \alpha^3}{\sqrt{T} m_e^3}, \quad (14)$$

where we imposed an infrared cutoff on the photon energy  $\omega > T$ , again corresponding to photons that can exchange  $\mathcal{O}(T)$  energy in a single scattering. If the pair annihilation and bremsstrahlung are both greater than the expansion rate at the beginning of the plasma evolution, right after most dark photons have decayed, those processes lead to a quick thermalization of the plasma. Since  $n_\gamma \ll T^3$ , these processes increase the total number density and decrease the temperature until  $T \leq m_e$  before any significant expansion, at which point both annihilation and bremsstrahlung rates decay exponentially due to the loss of leptons. For dark photon masses above  $\sim 10$  MeV, there is another possibility for rapid thermalization. Even if the pair annihilation rate is initially slower than the expansion, the energy loss rate due to bremsstrahlung [51]

$$\left. \frac{d \log \rho_e}{dt} \right|_{\text{brem}} = -\frac{8n_e \alpha^3}{m_e^2} \left( \text{Log} \left( \frac{2T}{e^{\gamma_E} m_e} \right) + \frac{5}{4} \right) \quad (15)$$

can be faster than that due to expansion

$$\left. \frac{d \log \rho_e}{dt} \right|_{\text{exp}} = -\frac{4\gamma}{r}, \quad (16)$$

where  $\rho_e = 3Tn_e$  is the energy density of the shell in the shell frame immediately after the dark photons decay. Energy loss due to bremsstrahlung leads to a quick decrease in the plasma temperature (but insignificant change to the lepton number density), which in turn increases the pair annihilation rate sufficiently to make it faster than the expansion. Afterwards, the evolution of the fireball is the same as in the case where both pair annihilation and bremsstrahlung were efficient already at the formation of the plasma.

The resulting photon spectrum (in the observer frame) is approximately thermal, with an apparent temperature given by  $\gamma_* T_*$ , where  $\gamma_*$  and  $T_*$  are respectively the plasma's Lorentz factor and temperature when it becomes optically thin for photons. The photon interaction rate drops exponentially once the plasma temperature is below  $m_e$  because the electron density becomes Boltzmann suppressed, leading to  $T_* \sim m_e/10$  with only a mild logarithmic sensitivity to the initial conditions of the plasma shell. In the thermalized scenario the temperature drops before the plasma expands significantly, and thus  $\gamma_* = \gamma_0 \lesssim 10$ , and effectively all of the energy radiated in dark photons gets converted into photons with energies in the 10 – 1000 keV range. The photon signal duration is set by light crossing time of the plasma shell, about 0.1-100 s depending on the dark photon parameters. The luminosity of the signal can be estimated by dividing the total energy output by the width of the plasma shell as shown in Eq. 8.

The parameter space region in which this thermal spectrum is generated is shown in Fig. 2 for two different assumptions about the duration of the remnant. It also shows the curve for which the total energy emitted in dark photons would be detectable at the Fermi gamma-ray burst monitor (GBM), assuming all of the energy gets converted to photons in the sensitivity range of the instrument (100 – 2000 keV) and a merger distance of 100 Mpc. Note that if the “fireball” is formed the dark photon energy would get certainly get converted to the GBM range because the initial boost  $\gamma_0$  is  $\mathcal{O}(1)$  for all relevant masses. This shows that one can probe most of the remaining parameter space above  $\epsilon \approx 10^{-11}$ , motivated by freeze-in dark matter scenarios, in the  $m' \approx 1 - 100$  MeV mass range by searching for these gamma-ray signals which coincide with a neutron star merger.

#### IV. DISCUSSION AND FUTURE PROSPECTS

The advanced LIGO/Virgo collaboration is currently sensitive to neutron star mergers within  $\sim 100$  Mpc of Earth [56]. The first BNS merger detection, GW170817, was about half this distance, and therefore unusually close given the estimated rate for BNS mergers. With some assumptions about the dynamics of the remnant of GW170817, one could in principle already constrain part of the dark photon parameter space in Fig. 2. However, distinguishing the signal from the GRB expected to be produced by the jet generated by the accretion into the newly formed black-hole will require further investigation. The expected dark photon signal is roughly thermal, and isotropic. With multiple observations of BNS merger spectra and light curves it should be possible to use these features and the signal duration to differentiate the dark photon flash from ordinary GRB. The LIGO/Virgo collaboration is projected to be sensitive to neutron star mergers as far away as  $\sim 200$  Mpc when it reaches design sensitivity in the next few years [57],

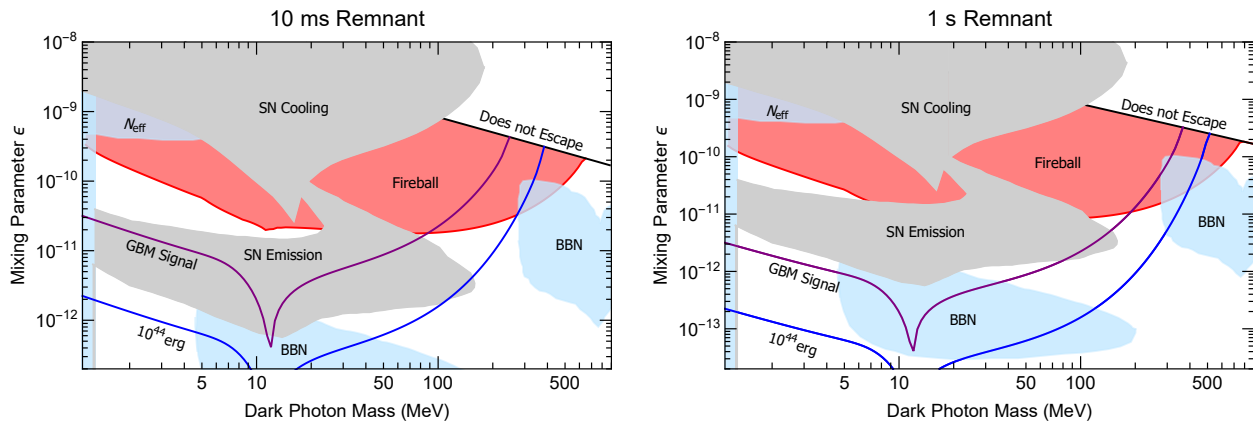


FIG. 2: Parameter space where dark photon signal generates an observable flash. The left plot shows the conditions produced when the merger emits dark photons for 10 ms, and the right plot shows the conditions produced when the merger produces dark photons for 1 s. The red region marks where the dark photons form a fireball which produces a bright thermal flash. Below the red region dark photons generate a dimmer non-thermal signal. The black line marks where the dark photon decay length is 1000 km. Dark photons that decay within 1000 km of the merger are assumed to get caught in the merger debris and not produce an observable signal. The purple line shows the minimum  $\epsilon$  needed to produce a signal visible to Fermi GBM for a merger 100 Mpc away ( $\sim 2 \times 10^{46}$  ergs). The blue line shows  $\epsilon$  needed to produce a  $10^{44}$  erg signal. The energy output scales approximately as  $\propto \epsilon^2$ . The gray and light blue regions show parameter space already ruled out by astrophysical [37, 39] and cosmological observations [35, 53–55]

at which point it will detect multiple mergers per year. With increased merger statistic, and utilizing more realistic remnant profiles, derived from simulations, to have a more robust prediction of the signal, we should be able to probe the parameter space in Fig. 2 that is above the purple line and within the fireball region. This will cover a large portion of the remaining parameter space motivated by dark matter freeze-in,  $\epsilon \gtrsim 10^{-11}$  [28].

In order to probe the parameter space where a fireball is not formed, there are two challenges that one must face. The first is that there are multiple processes that can produce photons from a dilute electron positron pair, which contribute to different parts of the photon spectrum. We leave the required detailed analysis for this to future work, but we expect that for part of the parameter space, the bulk of the signal will be in  $\sim 10$  MeV photons, for which we currently do not have very good coverage. There are a number of proposals such as e-ASTROGRAM [58], AMEGO [59], and MeVCube [60] that target the low MeV range which would significantly increase our reach to dark photons from BNS. The other challenge is that as the coupling decreases and the lepton density after the decay becomes very small, only a small fraction of the energy will be converted to photons, making the signal dimmer. One promising direction to overcome the decrease in photon luminosity is by using detectors with better angular resolution, which decreases the background to the signal. Future proposed mid-band detectors such as AMIGO [61], MAGIS [62], AION [63], ELGAR [64] should be able to detect BNS merger events in advance, allowing future more sensitive x-ray and gamma-ray telescopes with narrower fields of view to point to the relevant regions of the sky. These

telescopes can monitor the region where the merger is expected, and see the transient signal that would arise from dark photons formed in the merger, significantly enhancing the sensitivity to hard x-rays and MeV gamma-rays coming from the first seconds post merger.

We have shown that neutron star mergers can be used to probe dark sectors with unstable particles that decay to the standard model. We demonstrated this concept by studying the gamma-ray signatures that can arise from dark photon decay, and showed that this is a promising way to cover a large portion of unconstrained parameter space for the dark photon, including much of the remaining parameter space in which the interactions mediated by the dark photon can be responsible for producing the observed dark matter abundance. Utilizing the full potential of BNS as probes of dark sector will require a better understanding of the remnant dynamics and further investigation of how to distinguish the gamma-ray signal arising from dark sectors from the one generated by the relativistic jet responsible for the short GRB signal associated with mergers.

### Acknowledgements

The authors thank Tim Dietrich, Julian Krolik, and David Radice for useful discussions and Daniel Egaña-Ugrinovic for comments on the draft. GMT was supported in part by the NSF grants PHY-1914480, PHY-1914731, by the Maryland Center for Fundamental Physics (MCFP) and by the US-Israeli BSF Grant 2018236. MD was supported in part by NSF grant PHY-1818899.

- [1] B. P. Abbott et al. (LIGO Scientific, Virgo), *Phys. Rev. Lett.* **119**, 161101 (2017), 1710.05832.
- [2] B. P. Abbott et al. (LIGO Scientific, Virgo, Fermi GBM, INTEGRAL, IceCube, AstroSat Cadmium Zinc Telluride Imager Team, IPN, Insight-Hxmt, ANTARES, Swift, AGILE Team, 1M2H Team, Dark Energy Camera GW-EM, DES, DLT40, GRAWITA, Fermi-LAT, ATCA, ASKAP, Las Cumbres Observatory Group, OzGrav, DWF (Deeper Wider Faster Program), AST3, CAAS-TRO, VINROUGE, MASTER, J-GEM, GROWTH, JAGWAR, CaltechNRAO, TTU-NRAO, NuSTAR, Pan-STARRS, MAXI Team, TZAC Consortium, KU, Nordic Optical Telescope, ePESSTO, GROND, Texas Tech University, SALT Group, TOROS, BOOTES, MWA, CALET, IKI-GW Follow-up, H.E.S.S., LOFAR, LWA, HAWC, Pierre Auger, ALMA, Euro VLBI Team, Pi of Sky, Chandra Team at McGill University, DFN, ATLAS Telescopes, High Time Resolution Universe Survey, RIMAS, RATIR, SKA South Africa/MeerKAT), *Astrophys. J. Lett.* **848**, L12 (2017), 1710.05833.
- [3] B. P. Abbott et al. (LIGO Scientific, Virgo, Fermi-GBM, INTEGRAL), *Astrophys. J. Lett.* **848**, L13 (2017), 1710.05834.
- [4] J. J. Cowan, C. Sneden, J. E. Lawler, A. Aprahamian, M. Wiescher, K. Langanke, G. Martínez-Pinedo, and F.-K. Thielemann, *Rev. Mod. Phys.* **93**, 15002 (2021), 1901.01410.
- [5] P. Meszaros, *Ann. Rev. Astron. Astrophys.* **40**, 137 (2002), astro-ph/0111170.
- [6] E. Pian (2020), 2009.12255.
- [7] P. Mészáros, D. B. Fox, C. Hanna, and K. Murase, *Nature Rev. Phys.* **1**, 585 (2019), 1906.10212.
- [8] G. Camelió, T. Dietrich, S. Rosswog, and B. Haskell, *Phys. Rev. D* **103**, 063014 (2021), 2011.10557.
- [9] A. Endrizzi, A. Perego, F. M. Fabbri, L. Branca, D. Radice, S. Bernuzzi, B. Giacomazzo, F. Pederiva, and A. Lovato, *Eur. Phys. J. A* **56**, 15 (2020), 1908.04952.
- [10] D. Radice, *Symmetry* **12**, 1249 (2020), 2005.09002.
- [11] A. Perego, S. Bernuzzi, and D. Radice, *Eur. Phys. J. A* **55**, 124 (2019), 1903.07898.
- [12] D. Radice, A. Perego, K. Hotokezaka, S. A. Fromm, S. Bernuzzi, and L. F. Roberts, *Astrophys. J.* **869**, 130 (2018), 1809.11161.
- [13] S. Endlich, V. Gorbenko, J. Huang, and L. Senatore, *JHEP* **09**, 122 (2017), 1704.01590.
- [14] A. Hook and J. Huang, *JHEP* **06**, 036 (2018), 1708.08464.
- [15] L. Sagunski, J. Zhang, M. C. Johnson, L. Lehner, M. Sakellariadou, S. L. Liebling, C. Palenzuela, and D. Neilsen, *Phys. Rev. D* **97**, 064016 (2018), 1709.06634.
- [16] D. Croon, A. E. Nelson, C. Sun, D. G. E. Walker, and Z.-Z. Xianyu, *Astrophys. J. Lett.* **858**, L2 (2018), 1711.02096.
- [17] J. Huang, M. C. Johnson, L. Sagunski, M. Sakellariadou, and J. Zhang, *Phys. Rev. D* **99**, 063013 (2019), 1807.02133.
- [18] M. Bezares, D. Viganò, and C. Palenzuela, *Phys. Rev. D* **100**, 044049 (2019), 1905.08551.
- [19] J. A. Dror, R. Laha, and T. Opferkuch, *Phys. Rev. D* **102**, 023005 (2020), 1909.12845.
- [20] N. Sennett, R. Brito, A. Buonanno, V. Gorbenko, and L. Senatore, *Phys. Rev. D* **102**, 044056 (2020), 1912.09917.
- [21] T. Dietrich and K. Clough, *Phys. Rev. D* **100**, 083005 (2019), 1909.01278.
- [22] S. P. Harris, J.-F. Fortin, K. Sinha, and M. G. Alford, *JCAP* **07**, 023 (2020), 2003.09768.
- [23] B. Holdom, *Phys. Lett. B* **166**, 196 (1986).
- [24] M. Fabbrichesi, E. Gabrielli, and G. Lanfranchi (2020), 2005.01515.
- [25] R. Essig et al., in *Community Summer Study 2013: Snowmass on the Mississippi* (2013), 1311.0029.
- [26] J. Alexander et al. (2016), 1608.08632.
- [27] L. J. Hall, K. Jedamzik, J. March-Russell, and S. M. West, *JHEP* **03**, 080 (2010), 0911.1120.
- [28] X. Chu, T. Hambye, and M. H. G. Tytgat, *JCAP* **05**, 034 (2012), 1112.0493.
- [29] R. Essig, M. Fernandez-Serra, J. Mardon, A. Soto, T. Volansky, and T.-T. Yu, *JHEP* **05**, 046 (2016), 1509.01598.
- [30] S. Knapen, T. Lin, M. Pyle, and K. M. Zurek, *Phys. Lett. B* **785**, 386 (2018), 1712.06598.
- [31] O. Abramoff et al. (SENSEI), *Phys. Rev. Lett.* **122**, 161801 (2019), 1901.10478.
- [32] T. Aralis et al. (SuperCDMS), *Phys. Rev. D* **101**, 052008 (2020), [Erratum: *Phys.Rev.D* 103, 039901 (2021)], 1911.11905.
- [33] J. Redondo and M. Postma, *JCAP* **02**, 005 (2009), 0811.0326.
- [34] H. An, M. Pospelov, and J. Pradler, *Phys. Lett. B* **725**, 190 (2013), 1302.3884.
- [35] A. Fradette, M. Pospelov, J. Pradler, and A. Ritz, *Phys. Rev. D* **90**, 035022 (2014), 1407.0993.
- [36] D. Kazanas, R. N. Mohapatra, S. Nussinov, V. L. Teplitz, and Y. Zhang, *Nucl. Phys. B* **890**, 17 (2014), 1410.0221.
- [37] J. H. Chang, R. Essig, and S. D. McDermott, *JHEP* **01**, 107 (2017), 1611.03864.
- [38] E. Hardy and R. Lasenby, *JHEP* **02**, 033 (2017), 1611.05852.
- [39] W. DeRocco, P. W. Graham, D. Kasen, G. Marques-Tavares, and S. Rajendran, *JHEP* **02**, 171 (2019), 1901.08596.
- [40] E. Rrapaj and S. Reddy, *Phys. Rev. C* **94**, 045805 (2016), 1511.09136.
- [41] S. Bernuzzi et al., *Mon. Not. Roy. Astron. Soc.* **497**, 1488 (2020), 2003.06015.
- [42] S. Fujibayashi, S. Wanajo, K. Kiuchi, K. Kyutoku, Y. Sekiguchi, and M. Shibata, *Astrophys. J.* **901**, 122 (2020), 2007.00474.
- [43] D. Radice, S. Bernuzzi, and A. Perego, *Ann. Rev. Nucl. Part. Sci.* **70**, 95 (2020), 2002.03863.
- [44] A. Murguia-Berthier, E. Ramirez-Ruiz, F. De Colle, A. Janiuk, S. Rosswog, and W. H. Lee, *Astrophys. J.* **908**, 152 (2021), 2007.12245.
- [45] M. Shibata, E. Zhou, K. Kiuchi, and S. Fujibayashi, *Phys. Rev. D* **100**, 023015 (2019), 1905.03656.
- [46] M. Shibata, S. Fujibayashi, K. Hotokezaka, K. Kiuchi, K. Kyutoku, Y. Sekiguchi, and M. Tanaka, *Phys. Rev. D* **96**, 123012 (2017), 1710.07579.
- [47] M. Ruiz, S. L. Shapiro, and A. Tsokaros, *Phys. Rev. D* **97**, 021501 (2018), 1711.00473.
- [48] P. Meszaros, *Rept. Prog. Phys.* **69**, 2259 (2006), astro-ph/0605208.

- [49] T. Piran, Phys. Rept. **314**, 575 (1999), astro-ph/9810256.
- [50] R. Svensson, Astrophys. J. **258**, 321 (1982).
- [51] M. ALEXANIAN, Phys. Rev. **165**, 253 (1968).
- [52] E. Haug, Astronomy and Astrophysics **148**, 386 (1985).
- [53] J. R. Ellis, G. B. Gelmini, J. L. Lopez, D. V. Nanopoulos, and S. Sarkar, Nucl. Phys. B **373**, 399 (1992).
- [54] L. Zhang, X. Chen, M. Kamionkowski, Z.-g. Si, and Z. Zheng, Phys. Rev. D **76**, 061301 (2007), 0704.2444.
- [55] M. Ibe, S. Kobayashi, Y. Nakayama, and S. Shirai, JHEP **04**, 009 (2020), 1912.12152.
- [56] L. Instrument Science List, :, A. Buikema, C. Cahillane, G. L. Mansell, C. D. Blair, R. Abbott, C. Adams, R. X. Adhikari, A. Ananyeva, et al., arXiv e-prints arXiv:2008.01301 (2020), 2008.01301.
- [57] J. Aasi et al. (LIGO Scientific), Class. Quant. Grav. **32**, 074001 (2015), 1411.4547.
- [58] A. De Angelis et al. (e-ASTROGAM), Exper. Astron. **44**, 25 (2017), 1611.02232.
- [59] R. Caputo et al. (AMEGO) (2019), 1907.07558.
- [60] G. Lucchetta, M. Ackermann, R. Bühler, and F. Zappon, in *Space Telescopes and Instrumentation 2020: Ultraviolet to Gamma Ray*, edited by J.-W. A. den Herder, S. Nikzad, and K. Nakazawa, International Society for Optics and Photonics (SPIE, 2020), vol. 11444, pp. 834 – 843, URL <https://doi.org/10.1117/12.2561510>.
- [61] W.-T. Ni, G. Wang, and A.-M. Wu, Int. J. Mod. Phys. D **29**, 1940007 (2020), 1909.04995.
- [62] M. Abe, P. Adamson, M. Borcean, D. Bortoletto, K. Bridges, S. P. Carman, S. Chattopadhyay, J. Coleman, N. M. Curfman, K. DeRose, et al., arXiv e-prints arXiv:2104.02835 (2021), 2104.02835.
- [63] L. Badurina et al., JCAP **05**, 011 (2020), 1911.11755.
- [64] B. Canuel et al., Class. Quant. Grav. **37**, 225017 (2020), 1911.03701.

# Visible dark photon flashes from neutron star mergers

## Supplementary Material

Melissa Diamond and Gustavo Marques-Tavares

### I. DARK PHOTON PRODUCTION CALCULATION

The differential number flux of dark photons is given by:

$$\frac{dN}{dV dt} = \int d\omega \frac{dN}{dV dt d\omega} = \int \frac{d\omega \omega^2 v}{2\pi^2} e^{-\omega/T} (\Gamma'_{\text{abs},L} + 2\Gamma'_{\text{abs},T}) \quad (\text{S1})$$

Where  $\omega$  is the frequency of the dark photon,  $v$  is its velocity,  $\Gamma'_{\text{abs},L}$  is its longitudinal absorptive width, and  $\Gamma'_{\text{abs},T}$  is the absorptive width of the transverse mode. Inverse proton-neutron bremsstrahlung is the dominant absorption process so that will be the one considered here. Using the soft radiation approximation the absorptive width is given by [37, 40]

$$\Gamma'_{\text{ibr},L|T} = \frac{32}{3\pi} \frac{\alpha(\epsilon_m)^2 n_n n_p}{\omega^3} \left(\frac{\pi T}{m_N}\right)^{3/2} \langle \sigma_{np}^{(2)}(T) \rangle \left(\frac{m'}{\omega^2}\right)_L, \quad (\text{S2})$$

where  $n_n$  is the number density of neutrons,  $n_p$  is the number density of protons,  $m_N$  is the neutron mass,  $m'$  is the dark photon mass,  $T$  is the background temperature,  $\langle \sigma_{np}^{(2)}(T) \rangle$  is the proton neutron dipole scattering cross section,  $(\epsilon_m)^2$  is the in medium mixing angle and  $\left(\frac{m'}{\omega^2}\right)_L$  only applies to the longitudinal term and is 1 for the transverse polarizations. The cross section  $\langle \sigma_{np}^{(2)}(T) \rangle$  is taken from Ref. [40].

Plasma effects change the mixing between the photon and the dark photon. This can be described using an effective mixing parameter [37]

$$(\epsilon_m)_{L|T}^2 = \frac{\epsilon^2}{(1 - \text{Re}\Pi_{L|T}/m'^2)^2 + (\text{Im}\Pi_{L|T}/m'^2)^2} \quad (\text{S3})$$

Where  $\Pi$  is the polarization tensor. Its real component is given by:

$$\text{Re}\Pi_L = \frac{3\omega_p^2}{v^2} (1 - v^2) \left[ \frac{1}{2v} \ln\left(\frac{1+v}{1-v}\right) - 1 \right] \quad (\text{S4})$$

$$\text{Re}\Pi_T = \frac{3\omega_p^2}{2v^2} \left[ 1 - \frac{1-v^2}{2v} \ln\left(\frac{1+v}{1-v}\right) \right] \quad (\text{S5})$$

Here the velocity of the dark photon is determined by  $v = \sqrt{1 - \frac{m'^2}{\omega^2}}$ , and  $\omega_p$  is the plasma frequency, which for a gas of degenerate electrons is given by

$$\omega_p^2 = \frac{4\pi\alpha n_e}{\sqrt{m_e^2 + (3\pi^2 n_e)^{2/3}}}, \quad (\text{S6})$$

where  $m_e$  and  $n_e$  denote the electron mass and number density respectively.

Within the merger standard model photons are in local thermal equilibrium. Hence the imaginary part of the polarization becomes:

$$\text{Im}\Pi_{L|T} = -\omega \left(1 - e^{-\omega/T}\right) \Gamma_{\text{abs},L|T} \quad (\text{S7})$$

Where  $\Gamma_{\text{abs},L|T}$  is the absorptive width of the standard model photon, taken to be

$$\Gamma_{\text{ibr},L|T} = \frac{32\alpha}{3\pi} \frac{n_n n_p}{\omega^3} \left(\frac{\pi T}{m_N}\right)^{3/2} \langle \sigma_{np}^{(2)}(T) \rangle \left(\frac{m'}{\omega^2}\right)_L \quad (\text{S8})$$

$$\Gamma'_{\text{abs}} = (\epsilon_m)_{L|T}^2 \Gamma_{\text{abs}} \quad (\text{S9})$$



## II. ELECTRON POSITRON BREMSSTRAHLUNG

In this section we present the details for photon bremsstrahlung from electron positron scattering, which is the leading number changing process in the plasma formed after the dark photon decays. Following Ref. [51], we have that in a relativistic gas ( $T \gg m_e$ ) the differential bremsstrahlung rate from electron positron scattering is

$$\begin{aligned} \frac{dn_{\text{brem}}}{dt d\omega} &= 2n_e^2 r_0^2 \alpha e^{-\omega/T} \frac{d\omega}{\omega} \left[ \frac{28}{3} + 2\frac{\omega}{T} + \frac{\omega^2}{2T^2} + 2 \left( \frac{8}{3} + \frac{4\omega}{3T} + \frac{\omega^2}{T^2} \right) \log \frac{2T}{m_e e^{\gamma_E}} \right. \\ &\quad \left. - e^{-\omega/T} \text{Ei}(-\omega/T) \left( \frac{8}{3} - \frac{4\omega}{3T} + \frac{\omega^2}{T^2} \right) \right], \end{aligned} \quad (\text{S10})$$

where  $\gamma_E$  is the Euler-Mascheroni constant and Ei is the exponential-integral function. From this we find that

$$\begin{aligned} \frac{dn_{\text{brem}}}{dt} &\approx \frac{2n_e^2 r_0^2 \alpha}{9} \left[ 15 + 2\pi^2 - 84 \log(e^{\gamma_E} \omega_0/T) + 12 \log^2(e^{\gamma_E} \omega_0/T) \right. \\ &\quad \left. + 42 \log(2T/m_e e^{\gamma_E}) - 48 \log(2T/m_e e^{\gamma_E}) \log(e^{\gamma_E} \omega_0/T) \right], \end{aligned} \quad (\text{S11})$$

where  $\omega_0$  is the IR cutoff for the photon energy (the emission diverges at low photon energy due the well known soft divergence). In principle we should take  $\omega_0$  to be the lowest energy for which photons would still thermalize sufficiently quickly, in practice we will take it to be  $\omega_0 = m_e^2/T$ , which is the energy for which photons exchange on average  $T$  of energy within one collision with the electron bath. For a sufficiently relativistic plasma the double log enhanced emissions dominate and we can approximate

$$\frac{dn_{\text{brem}}}{dt} \approx \frac{2n_e^2 \alpha^3}{9m_e^2} \left[ 12 \log^2(e^{\gamma_E} m_e^2/T^2) - 84 \log(e^{\gamma_E} m_e^2/T^2) + 48 \log(e^{\gamma_E} m_e/T) \log(e^{\gamma_E} m_e^2/T^2) \right]. \quad (\text{S12})$$

For dark photon masses above  $\sim 10$  MeV, there is another possibility for rapid thermalization. Even if the pair annihilation rate is initially slower than the expansion, the energy loss rate due to Bremsstrahlung can be faster than that from expansion which leads to a quick decrease in the plasma temperature (but insignificant change to the lepton number density), which in turn increases the pair annihilation rate sufficiently to make it faster than the expansion. Afterwards, the evolution of the fireball is the same as in the case where both pair annihilation and bremsstrahlung were efficient from the beginning. Bremsstrahlung reduces the energy of the electrons and positrons in the shell by

$$\left. \frac{d \log \rho_e}{dt} \right|_{\text{brem}} = -\frac{8n_e \alpha^3}{m_e^2} \left( \text{Log} \left( \frac{2T}{e^{\gamma_E} m_e} \right) + \frac{5}{4} \right) \quad (\text{S13})$$

for relativistic plasmas. This energy loss is fast if it is larger than the energy loss due to expansion of the shell [51]

$$\frac{d \log \rho_e}{dt} = -\frac{4\gamma}{r}, \quad (\text{S14})$$

where we use  $\rho_e = 3Tn_e$ . This leads to a quick decrease in the temperature (but no change in  $n_e$  before annihilations become important), which in turn increases the annihilation rate. Because the annihilation rate increases as  $T^{-2}$  while the temperature decrease, but the energy loss rate is only log dependent on the temperature, the annihilation rate quickly becomes faster than both the energy loss rate and the expansion rate, which leads to a thermalized plasma.

## III. GRAVITATIONAL REDSHIFT

The number of dark photons emitted, their Lorentz factor upon decaying and the total energy stored in the expanding fireball shell will be altered by redshifting effects as the dark photons climb out of the gravitational well created by the merger remnant. To compute the exact impact of gravitational redshift on the signal requires a more accurate picture for the density profile of the remnant than the one we used to compute the signal. Redshifting will reduce the number of dark photons that escape the merger, and will reduce the total energy of the photos that do. Still assuming spherical symmetry, the number of dark photons that escape would now be found by taking

$$\frac{dN}{dt} = 4\pi \int_{r_{\text{min}}}^{r_{\text{max}}} \int_{\omega_m}^{\infty} \frac{d\omega \omega^2 v}{2\pi^2} e^{-\omega/T} (\Gamma_{\text{abs},L} + 2\Gamma_{\text{abs},T}), \quad (\text{S15})$$

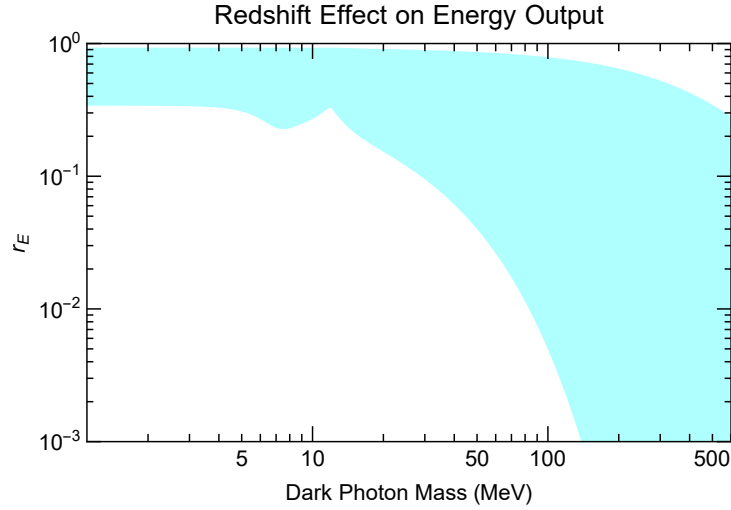


FIG. S1: Range of possible ratios between dark photon luminosity when redshifting effects are included and when such effects are neglected for a  $2.7M_{\odot}$  merger remnant. The upper limit for this ratio comes from a model which assumes the remnant has a constant density throughout of  $4 \times 10^{14} \text{ g cm}^3$ . The lower limit on this ratio comes from a model where the remnant has density of  $4 \times 10^{14} \text{ g cm}^3$  in the dark photon emission region (5 km-10 km from the center), with the remaining mass of the remnant stored in the inner 5 km. This strongly suppresses the dark photon luminosity because the amount of mass in the innermost region would be enough to form a black hole, preventing many dark photons from escaping.

Where  $\omega_m$  is the minimal energy a dark photon needs to escape the merger

$$\omega_m = \frac{m'}{\sqrt{1 - 2 \left( \frac{GM_{int}(r)}{r} \right)}} \quad (\text{S16})$$

$M_{int}(r)$  is the total mass contained within the radius  $r$  of the merger remnant. The total energy carried away by the dark photons can be found using

$$\frac{dE}{dt} = 4\pi \int_{r_{min}}^{r_{max}} \int_{\omega_m}^{\infty} \frac{d\omega \omega^3 \sqrt{1 - 2 \left( \frac{GM_{int}(r)}{r} \right)} v}{2\pi^2} e^{-\omega/T} (\Gamma_{\text{abs},L} + 2\Gamma_{\text{abs},T}) \quad (\text{S17})$$

The average energy,  $E_{ave}$  is then found by dividing the total energy output after accounting for redshifting by the total number of dark photons that successfully escape the merger. In Fig. S1 we show the approximate range of the ratio between the dark photon luminosity when redshifting effects are considered and when such effects are neglected for a  $2.7M_{\odot}$  merger remnant,  $r_E$ . The upper bound of this ratio is for a model that assumes the remnant has a constant density of  $4 \times 10^{14} \text{ g cm}^{-3}$  throughout, extended out to a radius such that the total mass is  $2.7M_{\odot}$ . The lower bound is set by a model where the remnant has a density of  $4 \times 10^{14} \text{ g cm}^{-3}$  in the emission region (between 5 km and 10 km from the merger center), no density in the region beyond 10 km from the core, and the remaining mass of the  $2.7 M_{\odot}$  remnant residing in the inner 5 km of the remnant. Most models of merger remnants have similar densities to those used here in the emission region, and become more dense closer to the core [9–11, 41], however the density in the lower curve is so large that it would already be a black-hole which is not the case for the simulations. The first model underestimates the central region's density and thus leads to a shallower gravitational potential. The second model, on the other hand, significantly overestimates the density in the central region, leading to a large escape velocity and thus a significant decrease in luminosity due to gravitational redshifting. The figure shows how sensitive to the density modeling this effect is, specially when considering dark photon masses larger than the remnants temperature. The real effect, using a more realistic density profile, will be somewhere in between the two limiting cases, but would primarily affect the large mass end of the plot.